Chen
EURASIP Journal on Advances in Signal Processing (2023) 2023:129
https://doi.org/10.1186/s13634-023-01084-1

EURASIP Journal on Advances in Signal Processing

RESEARCH Open Access

Multi-user communications for line-of-sight large intelligent surface systems

Jiayi Chen[1*]

*Correspondence: chenjiayi@szu.edu.cn

[1] College of Electronics and Information Engineering, Shenzhen University, Shenzhen, Guangdong Province, China

Abstract

In this paper, we propose a new interference-suppression beamformer design and a Direction-of-Arrival (DoA) estimation method for Line-of-Sight (LoS) multi-user communication systems with circular Large Intelligent Surfaces (LISs). This symmetrical circular-shaped LIS allows signals defined on it to be formed by combining Fourier and Bessel series. The Fourier harmonics are orthogonal along the rotational direction and the Bessel functions constituting the Bessel series are orthogonal along the radial direction. Synthesizing basis functions from these two series results in the proposed interference-suppression beamformer, with their coefficients designed to cancel inter-user interference. Also by exploiting signal structure of a circular LIS communicating with Mobile Stations (MSs), we devise a DoA estimation method to obtain directional information of incoming signals. Under LoS channel, the DoA corresponds to elevation and Azimuth angles of MSs relative to the LIS. This method is numerically demonstrated to have promising performance with high-frequency carriers.

Keywords: Large intelligent surface, Fourier–Bessel series, Interference-suppression, DoA estimation

1 Introduction

Large Intelligent Surface (LIS) is a spatial continuous aperture packed with a large number of antennas [1]. Several advantages that help improving existing wireless communication systems come with this new configuration. First, the continuous aperture of a LIS enables fine tuning of electromagnetic fields on the surface. This provides flexibilities in designing beamformers to achieve spatial diversities. Second, a continuous aperture can focus transmitting energy on a small area with high spatial resolution. This property not only can boost transmission efficiency, but also is favorable in precise positioning and wireless charging. Third, LIS-based systems can achieve high energy efficiency with its surface structure for transmitting and receiving signals, as shown in [1–3]. Fourth, utilizing advanced metamaterial technology, LISs can be installed integrating with surfaces such as windows, walls, and advertising boards on streets and high-ways [4]. These advantages coupled with recent developments of metamaterials and programmable metasurfaces that makes implementing a practical LIS system possible [5–9], has promoted LIS as a promising technology to serve future wireless communication systems with ever-increasing demand of high-speed, high-volume data transmissions [2, 3, 10].

In existing literature, LISs can be used in either of the following two ways. The first is to use LIS as a constructive signal reflector so that the composite channel between a transmitter and a receiver becomes favorable. This is also known as *Reconfigurable Intelligent Surface (RIS)* or *Intelligent Reflecting Surface (IRS)* [7, 11–13]. The second is to use LIS as a transmitter and/or receiver. In this paper, we refer to LIS as in the second way.

One fundamental problem about LIS systems is what capacity they can achieve. This line of researches is conducted by applying electromagnetic theory to model propagation channels between two transmitting/receiving LIS volumes/surfaces. Then, the Degree-of-Freedoms (DoFs), which can be interpreted as the number of orthogonal channels or communication modes, are obtained by solving for the number of eigenfunctions of the channel. In [14], the authors obtain a formal solution of orthogonal modes between one transmitting volume and one receiving volume communicating in free space. Specifically, the result is applied to calculate concrete communication modes between two volumes with rectangular shape. Asymptotic DoFs for two communicating LISs are derived in [4]. The result shows that larger-than-one DoF can be achieved in Line-of-Sight (LoS) channel condition, showcasing the possible benefit of deploying LIS systems. Authors in [15] take effects of multipath channel into account by incorporating an experimental scattering channel model in their analysis of DoF for systems with transmit and receive antenna arrays. The resulting spatial DoF is the product of effective array aperture and angular spread of the physical channel using spherical uni-polarized antenna arrays. These theoretical results provides insightful observations for designing LIS systems. Under practical channel condition, solving for orthogonal communication modes is a challenge task because it involves complex differential equations, which is usually complicated to solve. As an effort to address this challenge, authors in [16] propose a practical method for deriving near-field communication modes between linear aperture antennas in free space.

Another line of LIS-related researches includes performance analysis and transceiver design. In [3], the asymptotic capacity per unit-volume as well as DoF are analyzed for one- and two-dimensional (rectangular) LISs with matched-filter receivers, showing the promising advantages of the system for data transmission. In [17], positioning using LIS is investigated and Cramer-Rao bounds are computed under various scenarios. These two seminal works investigate the possibilities of LISs as a new technology for communications and positioning. In [2], authors consider circular-shaped LISs communicating in the uplink, and calculate array gain, spatial resolution and capacity. This work first explore the effect of shape in implementing a LIS system. Performance of LIS system under practical channel environments with channel estimation error and hardware impairments is studied in [18, 19]. Asymptotic rates are analyzed and channel hardening effects discussed. This study shows benefits of LIS under practical channel, but does not propose new transceiver schemes. In [20], authors propose a channel model taking mutual coupling, superdirectivity and near-field effects into account, and develop matched filter and weighted MMSE receivers for this model. In [21], authors ultilize electromagnetic information theory to formulate the continuous-aperture-MIMO pattern function design problem into an projection optimization problem by projecting continuous functions on finite orthogonal bases.

As can be seen from the above survey, most existing literatures study performance of Matched Filter (MF) or Minimum Mean-Square Error (MMSE) transceivers applied to LIS systems. These conventional techniques might as well be employed in LIS systems. However, they do not exploit all specific features of channels and transmitting signals of a LIS system. First, LIS is usually studied under LoS channels. Indeed, this is a reasonable channel model for LIS systems, as is argued in [3]. On one hand, LIS surfaces are deployed high up on top of buildings, resulting in dominant LoS path to Mobile Stations (MSs). On the other hand, employment of high-frequency spectrum such as millimeter wave, due to high-capacity demands and spectrum scarcity, also leads to LoS predominant propagations [22]. Under LoS model, channel coefficients are related to parameters such as Direction-of-Arrival (DoA) and the relative distance between transmitters and receivers. These parameters are implied in the signal structure, which might be exploited for transceiver design. Second, LIS can be manufactured in different shapes. Symmetric ones such as circular are preferable as spatial harmonics, e.g., Fourier series, can be defined on them. These harmonics provide a set of bases to synthesize signal waveforms. Third, LISs are continuous apertures, which is more mathematically tractable than discrete configurations (e.g., Massive MIMO). Inspired by these observations, we propose a new transceiver design method for multi-user LIS systems.

In this paper, we consider circular LISs communicating with multiple MSs in LoS channel. Exploiting the symmetric property of a circular LIS, we can synthesize Bessel and Fourier series defined on it to achieve interference-free communications. Although [2] also studies circular LIS, we are different in terms of main content and methodology. The majority of [2] is on analysis of spectrum efficiencies and properties of LIS systems, while this paper focus on methods of designing multi-user transceiver and estimating DoA. In terms of methodology, we adopt new analysis techniques and propose new transceiver design method.

Our contributions in this paper can be summarized as follows.

- We develop a new analysis of performance of LIS with MF transceiver. The analysis reveals a new observation of the inter-user interference terms. The strength of this interference is not determined by physical inter-user distance, as is conventionally believed, but by projected distance (see Sect. 3).
- We propose a new interference-suppression transceiver based on Bessel-and-Fourier–Series Synthesis (BFSS). The orthogonal Bessel series form a basis for signals along the radial direction and the Fourier series for signals along the rotational direction. By combining these two and tuning coefficients of the synthesized series, we obtain a beamformer that suppresses interference. The proposed beamformer is also numerically demonstrated to perform well in high Signal-to-Noise Ratio (SNR) regime.
- We propose a new DoA estimation method to obtain directional information of signals coming from a MS. Under LoS channels, the estimated DoAs are elevation and azimuth angles of a MS with respect to the LIS. We numerically demonstrate the promising performance of the proposed estimation method for carrier frequency in mmWave spectrum and higher.

The rest of the paper are organized as follows. System model and preliminary introduction of spatial harmonics are presented in Sect. 2. New interference-suppressing beamformer is proposed in Sect. 3 along with an analysis of MF transceiver. DoA estimation method is presented in Sect. 4. Numerical results are shown and analyzed in Sect. 5. Conclusions are drawn in Sect. 6.

1.1 Notation and definition

In this paper, boldface upper- and lower-case symbols represent matrices and vectors, respectively. The identity matrix is $\mathbf{I}$ without specifying its size, as it is clear from context. The conjugate, transpose, and Hermitian transpose operators are denoted by $(\cdot)^*$, $(\cdot)^T$, and $(\cdot)^H$, respectively. Component-wise multiplication is denoted by $\odot$. Expectation operation and absolute value are represented by $\mathbb{E}[\cdot]$ and $|\cdot|$, respectively. The norm of a vector $\mathbf{x}$ is denoted by $\|\mathbf{x}\|$. span($\mathbf{A}$) means a linear space spanned by columns of matrix $\mathbf{A}$.

2 System model

As shown in Fig. 1, we consider a base station equipped with a circular LIS of radius R, denoted by $\mathcal{D}$, situated on the $x-y$ plane, with its center at the origin o of a 3-D coordinate system. The LIS communicates with K MSs situated in front of it. Denote the kth ($k = 1, 2, \cdots, K$) MS's position at M_k with spherical coordinate represented by $(\rho_k, \theta_k, \gamma_k)$, where ρ_k is the distance from MS k to the coordinate origin o, θ_k is the elevation angle, measured with respect to the z axis and γ_k the azimuth angle, measured counterclockwise with respect to the x-axis. All MSs are equipped with single antenna.

2.1 Channel model

In practical deployment, LISs can be installed outside the wall of a top building, covering MSs roaming down on streets. The distance between a LIS and a MS is usually much larger than the size of a LIS, and the signal is dominated by Line-of-sight (LoS) component. In this paper, a far-field LoS propagation channel is assumed with $\rho_k \gg R$,

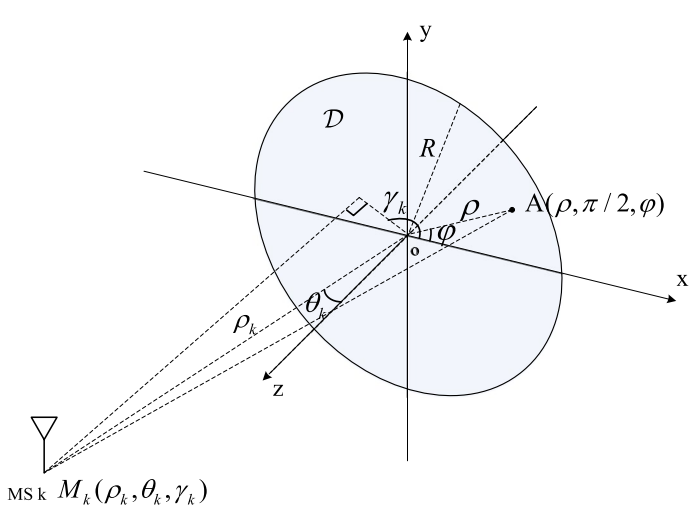

Fig. 1 LIS model

$k = 1, 2, \cdots, K$, and ρ_k is also larger than the Rayleigh distance $2(2R)^2/\lambda$ [2]. Consider an arbitrary infinitesimal element $A \in \mathcal{D}$ (on $x - y$ plane) on the LIS with coordinate $(\rho, \pi/2, \varphi)$. The channel coefficient between A and M_k can be modeled as [2, 23, 24]

$$g_k(\rho, \varphi) = \frac{\lambda}{4\pi |M_k - A|} h_k(\rho, \varphi) \approx \frac{\lambda}{4\pi \rho_k} h_k(\rho, \varphi), \tag{1}$$

where λ is the carrier wavelength. Also note that path-loss factor in the above equation can be well approximated as $\frac{1}{|M_k - A|} \approx \frac{1}{\rho_k}$ for $A \in \mathcal{D}$, since $\rho_k \gg R$. The channel's effect on phase is accounted for by $h_k(\rho, \varphi)$, which is given by

$$h_k(\rho, \varphi) = e^{-j\frac{2\pi}{\lambda}|M_k - A|}. \tag{2}$$

The approximation of $|M_k - A|$ by ρ_k in (1) is too crude to be applied to the phase term in the above equation. A second-order approximation is needed here to take into account of phase variations on $\mathcal{D}$.

$$\begin{aligned} |M_k - A| &= \sqrt{\rho_k^2 - 2\rho_k \rho \sin(\theta_k)\cos(\varphi - \gamma_k) + \rho^2} \\ &\approx \rho_k - \rho \sin(\theta_k)\cos(\varphi - \gamma_k). \end{aligned} \tag{3}$$

Equation (3) is obtained by omitting second and higher order terms due to $\rho_k \gg \rho$ for $\rho \leqslant R$. It can be seen that the first term in (3) is constant for all $A \in \mathcal{D}$. The phase shift it induced can be compensated by each MS, thus this term can be omitted for succinct expressions. From here on, $h_k(\rho, \varphi)$ is expressed in polar coordinate as

$$h_k(\rho, \varphi) = e^{j\frac{2\pi}{\lambda}\rho \sin(\theta_k)\cos(\varphi - \gamma_k)}. \tag{4}$$

2.2 Signal model

The LIS transmits signal s_k intended for MS k, precoded by filter $f_k(\rho, \varphi)$. The transmitted signals are zero-mean and independent of each other, i.e.,

$$\mathbb{E}[s_k] = 0, \tag{5}$$

$$\mathbb{E}[s_k^* s_k] = P_k, \tag{6}$$

$$\mathbb{E}[s_i^* s_j] = 0, \quad \forall i \neq j. \tag{7}$$

The received signal at the l-th MS is a summation of signals from all of $\mathcal{D}$, which can be written as

$$r_l = \int_{\mathcal{D}} g_l(\rho, \varphi) \sum_{k=1}^{K} f_k(\rho, \varphi) s_k \rho d\rho d\varphi + n_l, \tag{8}$$

for $l = 1, \cdots, K$. The filters $f_k(\rho, \varphi)$ are normalized to have unit power. The noise term is a additive white Gaussian noise with mean zero and variance σ_l^2. Note that this noise is an average of noises of elements on the LIS.

2.3 Orthogonal bessel series

This section briefly introduces orthogonal Bessell series and related expressions that will be used in later sections.

A circular LIS, like the one shown in Fig. 1, possesses rotational symmetry as well as radial symmetry. Signals defined on domains with circular symmetry can be decomposed into circular harmonics of integer frequencies, i.e., Fourier series. Along the radial direction, it is natural to decompose electromagnetic signals into orthogonal Bessel series as in [25, 26].

An orthogonal Bessel series is of the form [26]

$$\bar{f}(\rho) = \sum_{n=1}^{\infty} c_n J_\nu(a_{\nu n}\rho/R), \quad 0 \leqslant \rho \leqslant R,\ \nu > -1, \tag{9}$$

where $a_{\nu n}$ denotes the n-th zero of ν-th order Bessel function $J_\nu(\cdot)$ of the first kind, i.e., $J_\nu(a_{\nu n}) = 0$, and c_n the series coefficients. In the decomposition, the Bessel functions with different zeros in their arguments are orthogonal, as the following orthogonality equation shows.

$$\int_0^R \rho J_\nu(a_{\nu n}\rho/R) J_\nu(a_{\nu m}\rho/R) d\rho = 0, \quad \forall n \neq m. \tag{10}$$

By this orthogonal property, the coefficients c_n can be obtained as

$$c_n = \frac{2}{R^2[J_{\nu+1}(a_{\nu n})]^2} \int_0^R \bar{f}(\rho) J_\nu(a_{\nu n}\rho/R)\rho d\rho. \tag{11}$$

In the above equation, the factor $\frac{2}{R^2[J_{\nu+1}(a_{\nu n})]^2}$ is to normalize the result, since

$$\int_0^R [J_\nu(a_{\nu n}\rho/R)]^2 \rho d\rho = R^2[J_{\nu+1}(a_{\nu n})]^2/2. \tag{12}$$

Utilizing Bessel series along radial direction and Fourier harmonics along rotational direction, we can synthesize beamforming patterns with desirable properties. Based on this observation, we will investigate into designing interference-suppressing transceiver in next section.

3 Bessel-and-Fourier series synthesis (BFSS) transceiver

In this section, we first develop a new analysis of MF transceiver, and then propose the design of a interference-suppressing transceiver for multi-user LIS systems.

3.1 MF transceiver

As is well known, MF maximizes individual receiver's signal power, ignorant of inter-user interference. For MS k, its MF transmit filter is given by

$$f_k^{(MF)}(\rho, \varphi) = \frac{1}{\sqrt{\pi}R} h_k^*(\rho, \varphi), \tag{13}$$

where $\frac{1}{\sqrt{\pi}R}$ is a normalization factor to keep the filter power being 1 when integrating over the LIS. The received signal for MS l can then be obtained as

$$\begin{aligned} r_l &= \int_{\mathcal{D}} g_l(\rho,\varphi) \sum_{k=1}^{K} f_k^{(MF)}(\rho,\varphi) s_k \rho d\rho d\varphi + n_l \\ &= \frac{\tau_l}{2} s_l + \tau_l \sum_{k\neq l} \Phi_{lk} s_k + n_l, \end{aligned} \tag{14}$$

where $\tau_l = \frac{\lambda R}{2\sqrt{\pi}\rho_l}$. The received signal consists of the desired signal for MS l, the inter-user interference and the noise. The *normalized effective channel coefficient* Φ_{lk} in the inter-user interference term is given by

$$\Phi_{lk} \triangleq \frac{1}{2\pi R^2} \int_{\mathcal{D}} h_l(\rho,\varphi) h_k^*(\rho,\varphi) \rho d\rho d\varphi. \tag{15}$$

This coefficient signifies inter-user interference level and its analytical expression is obtained in the following proposition.

Proposition 1 *The normalized effective channel coefficients Φ_{lk} are calculated as*

$$\Phi_{lk} = \frac{J_1(2\pi R\Delta(k,l)/\lambda)}{2\pi R\Delta(k,l)/\lambda}, \tag{16}$$

where the projected distance $\Delta(k,l)$ between MS k and l is calculated as

$$\Delta(k,l) = \sqrt{\sin^2\theta_k + \sin^2\theta_l - 2\sin\theta_k \sin\theta_l \cos(\gamma_k - \gamma_l)}. \tag{17}$$

Proof See Appendix A. □

Remark 1

Note that the result obtain in Proposition 1 is the same as that in [2], only differing in a constant phase factor. This factor is pre-compensated as explained in Sect. 2.1 (after (3)), resulting in succinct expressions without restricting the applicability of our result. Note that the derivation of the normalized effective channel coefficient Φ_{lk}, as shown in Appendix A, is different from [2]. This result leads to a physical interpretation of the variable $\Delta(k,l)$ in its argument. We see from (17) that $\Delta(k,l)$ is the distance of two points $(\sin\theta_k, \gamma_k)$ and $(\sin\theta_l, \gamma_l)$ on the $x-y$ plane. These two points are projections of MS k and l's locations, i.e., $(\rho_k, \gamma_k, \theta_k)$ and $(\rho_l, \gamma_l, \theta_l)$, onto the $x-y$ plane and normalized by their, respectively, distance from origin o.

Note that when two MSs' projected positions on $x-y$ plane are very close, i.e., $\Delta(k,l) \to 0$, we have

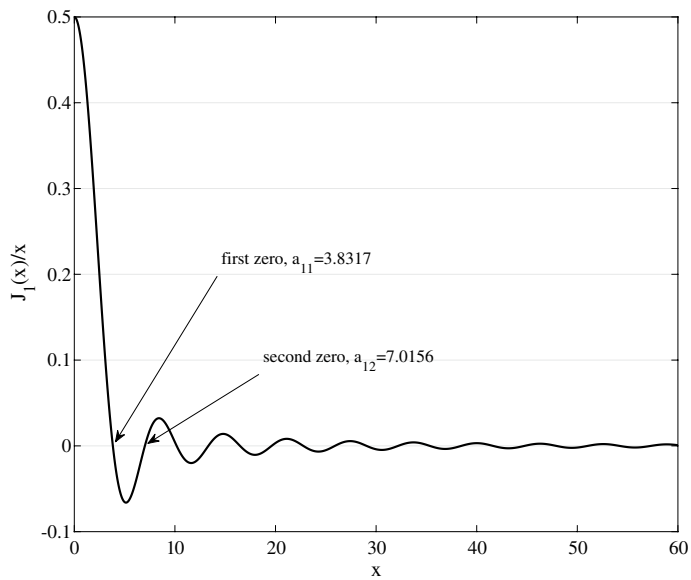

Fig. 2 A plot of function $\frac{J_1(x)}{x}$. The main lobe width is equal to the first zero of Bessel function $J_1(x)$, which is approximately $a_{11} \approx 3.8317$

$$\begin{aligned}\lim_{\Delta(k,l)\to 0} \Phi_{lk} &= \lim_{\Delta(k,l)\to 0} \frac{\lambda}{2\pi R\Delta(k,l)} J_1\left(\frac{2\pi R\Delta(k,l)}{\lambda}\right) \\ &= \frac{1}{2}[J_0(0) - J_2(0)] \\ &= \frac{1}{2},\end{aligned} \tag{18}$$

where the derivative of Bessel function $J_1(x)$ is utilized, i.e., $J_n'(x) = \frac{1}{2}[J_{n-1}(x) - J_{n+1}(x)]$. This channel coefficient achieves maximum value when $\Delta(k,l) = 0$ (ref. to Fig. 2).

The normalized channel coefficient is a function of projected distance between different MSs. When two MSs' projected positions overlapped, the received inter-user interference reaches maximum power level, the same as the power of the desired signal component, as seen from (14). This is the case when two MSs locate on the same radial from the origin o (with the same elevation and azimuth angles). This means one MS is behind the other one as seen from o, which is very unlikely since we consider LoS path and MSs are usually roaming on a surface under the LIS.

Based on Eq. (14), we derive the sum rate for MF transmitter as shown in the following proposition.

Proposition 2 *The sum rate for MF transceiver is given by*

$$\mathcal{C}^{(MF)} = \sum_{l=1}^{K} \log\left(1 + \frac{P_l R^2 \lambda^2/(4\sqrt{\pi}\rho_l)^2}{\sum_{k\neq l} \Phi_{lk}^2 P_k R^2 \lambda^2/(2\sqrt{\pi}\rho_l)^2 + \sigma_l^2}\right). \tag{19}$$

From the above analysis, we see that the sum rate is dependent on normalized effective channel coefficients Φ_{lk} between interfering terminals. These coefficients are closely related to the projected distance $\Delta(k,l)$ between two interfering MSs. The envelop of

Φ_{lk} decreases as $\Delta(k,l)$ increases as seen from Fig. 2. Spatial proximity of MSs results in large interference, especially when two MSs situated on the same line going through the origin of the LIS.

If all MSs have the same power constraint, we have the following corollary.

Corollary 1 *For equal power transmissions, i.e., $P_k = P,\ \forall k$, the sum rate can be written as*

$$\mathcal{C}^{(MF)} = \sum_{l=1}^{K} \log\left(1 + \frac{1/4}{\sum_{k\neq l}\Phi_{lk}^2 + 1/\varrho_l}\right), \tag{20}$$

where $\varrho_l = \frac{PR^2\lambda^2}{4\pi\rho_l^2\sigma_l^2}$. And

$$\mathcal{C}^{(MF)} \to \sum_{l=1}^{K} \log\left(1 + \frac{1}{4\sum_{k\neq l}\Phi_{lk}^2}\right), \quad \text{as } \varrho_l \to \infty. \tag{21}$$

At high SNR, sum rate is dominantly determined by normalized effective channel coefficients Φ_{lk}, which are functions of the radius R of the LIS and carrier wavelength λ, as seen from (16). An interesting observation is that, given other conditions the same, increasing R or decreasing λ decreases the normalized effective channel coefficients and thus inter-user interferences. In consequence, the sum rate increases. This is the case because inter-user distance affects interference through its normalization by carrier wavelength. Smaller wavelength results in large normalized inter-user distance. Another observation is that the sum rate saturates at high SNR, as (21) shows. This is due to the MF transceiver not considering suppressing inter-user interference.

3.2 BFSS transceiver

Inter-user interference is a major cause of performance degradation in future wireless communication systems with massive connections sharing a same spectrum. To mitigate inter-user interference, new transceivers have to be designed for LIS systems. In the following, we develop a interference-suppressing transceiver by synthesizing Bessel and Fourier series defined on the LIS.

Denote by $f_k^{(\mathrm{BFSS})}(\rho,\varphi)$ the BFSS filter for MS k. We consider interference-mitigating beamformer of the following form

$$\begin{aligned} f_k^{(\mathrm{BFSS})}(\rho,\varphi) =& h_k^*(\rho,\varphi)\sum_{m=1}^{\infty} c_{km} J_\nu\left(a_{\nu m}\frac{\rho}{R}\right)e^{j(m-1)\varphi}, \\ & 0 \leqslant \rho \leqslant R, \quad \nu > -1, \end{aligned} \tag{22}$$

where $a_{\nu m}$ is defined in (9).

Remark 2

Note that in Eq. (22), only Fourier harmonics of nonnegative frequencies are included, i.e., $e^{j(m-1)\varphi}$, for $m = 1, 2\cdots$. As a result, the synthesized signals do not represent all possible signals that can be formed when employing all of available harmonics. This will not

restrict our design of transceiver that follows. As it turns out, it is enough for the purpose of a interference suppression transceiver.

The filter coefficients c_{km} in (22) are to be designed such that the following normalization conditions are satisfied

$$\sum_{m=1}^{\infty}(c_{km}\beta_m)^2 = 1, \quad \forall\, k, \tag{23}$$

where $\beta_m = \sqrt{\pi}RJ_{\nu+1}(a_{\nu m})$. Using $f_k^{(\mathrm{BFSS})}(\rho,\varphi)$, the received signal at MS l can be written as

$$r_l = \int_{\mathcal{D}} g_l(\rho,\varphi)\sum_k f_k^{(\mathrm{BFSS})}(\rho,\varphi)s_k\rho d\rho d\varphi + n_l \tag{24}$$

We summarize the resulting formula for signal r_l in the following proposition.

Proposition 3 *The received signal r_l can be rewritten as*

$$r_l = \frac{\lambda}{2\rho_l}c_{l1}\xi_0 s_l + \frac{\lambda}{2\rho_l}\sum_{k\neq l}s_k\sum_{m=1}^{M}c_{km}\zeta_{lkm} + n_l, \tag{25}$$

where

$$\xi_0 = \frac{R^2}{a_{01}}J_1(a_{01}), \tag{26}$$

and

$$\begin{aligned}\zeta_{lkm} &= j^{m-1}e^{j(m-1)\alpha_{kl}}\\ &\times\int_0^R J_0\left(a_{0m}\frac{\rho}{R}\right)J_{m-1}\left(\frac{2\pi}{\lambda}\rho\Delta(k,l)\right)\rho d\rho \quad \text{for } k\neq l,\end{aligned} \tag{27}$$

and α_{kl} is defined as

$$\alpha_{kl} \triangleq \arctan\left\{\frac{\sin\theta_l\sin\gamma_l - \sin\theta_k\sin\gamma_k}{\sin\theta_l\cos\gamma_l - \sin\theta_k\cos\gamma_k}\right\}. \tag{28}$$

Proof See Appendix B. □

To suppress inter-user interference, we set the undetermined coefficients c_{km} such that the following system of linear equations are satisfied

$$\sum_{m=1}^{M}c_{km}\zeta_{lkm} = 0, \quad l = 1,2,\cdots,K,\ l\neq k, \tag{29}$$

for $k = 1,2,\cdots,K$. The above equations can be written in matrix form as

$$\Pi_k \mathbf{c}_k = \mathbf{0}, \tag{30}$$

where

$$\mathbf{c}_k = [c_{k1} \;\; c_{k2} \;\; \cdots \;\; c_{kM}]^T, \tag{31}$$

$$\Pi_k = \begin{bmatrix} \zeta_{1k1} & \zeta_{1k2} & \cdots & \zeta_{1kM} \\ \vdots & \vdots & \ddots & \vdots \\ \zeta_{(k-1)k1} & \zeta_{(k-1)k2} & \cdots & \zeta_{(k-1)kM} \\ \zeta_{(k+1)k1} & \zeta_{(k+1)k2} & \cdots & \zeta_{(k+1)kM} \\ \vdots & \vdots & \ddots & \vdots \\ \zeta_{Kk1} & \zeta_{Kk2} & \cdots & \zeta_{KkM} \end{bmatrix}. \tag{32}$$

The solution $\mathbf{c}_k$ is in the null space of Π_k,

$$\mathbf{c}_k \in \operatorname{span}\Big(\mathbf{I} - \Pi_k^\dagger (\Pi_k \Pi_k^\dagger)^{-1} \Pi_k\Big). \tag{33}$$

Proposition 4 *The BFSS filter coefficients* $\mathbf{c}_k$ *are chosen according to* (33). *The maximum SNR achieved by MS k is given by*

$$\begin{aligned} &\mathrm{SNR}_k^{(\mathrm{BFSS})} \\ &= \frac{P_k \lambda^2 \xi_0^2}{4\rho_k^2 \sigma_k^2} \left(\frac{\mathbf{e}_1^\dagger \big(\mathbf{I} - \Pi_k^\dagger (\Pi_k \Pi_k^\dagger)^{-1} \Pi_k\big) \mathbf{e}_1}{\big\| \big[\big(\mathbf{I} - \Pi_k^\dagger (\Pi_k \Pi_k^\dagger)^{-1} \Pi_k\big) \mathbf{e}_1 \big] \odot \mathbf{b} \big\|} \right)^2, \end{aligned} \tag{34}$$

where $\mathbf{e}_1 = [1 \; 0 \; \cdots \; 0]^T$ *and* $\mathbf{b} = [\beta_0 \;\; \beta_1 \;\; \cdots \;\; \beta_M]^T$ (*ref. to* (23)). *The sum rate achieved is given by*

$$\mathcal{C}^{(\mathrm{BFSS})} = \sum_{k=1}^{K} \log\Big(1 + \mathrm{SNR}_k^{(\mathrm{BFSS})}\Big). \tag{35}$$

Proof The coefficients can be obtained by picking one vector from the above null space and normalized. Of these solutions, the one with maximum c_{k1} is desirable, since it's a gain of the desirable signal component in MS k' received signal. This can be achieved by projecting vector $\mathbf{e}_1 = [1 \; 0 \; \cdots \; 0]^T$ onto the null space, resulting in $\big(\mathbf{I} - \Pi_k^\dagger (\Pi_k \Pi_k^\dagger)^{-1} \Pi_k\big) \mathbf{e}_1$. Taking the normalization condition (23) into account, we have

$$\max c_{k1} = \frac{\mathbf{e}_1^\dagger \big(\mathbf{I} - \Pi_k^\dagger (\Pi_k \Pi_k^\dagger)^{-1} \Pi_k\big) \mathbf{e}_1}{\big\| \big[\big(\mathbf{I} - \Pi_k^\dagger (\Pi_k \Pi_k^\dagger)^{-1} \Pi_k\big) \mathbf{e}_1 \big] \odot \mathbf{b} \big\|}, \tag{36}$$

where $\mathbf{b} = [\beta_0 \;\; \beta_1 \;\; \cdots \;\; \beta_M]^T$. □

From (35), it can be seen that sum rate grows linearly with SNR in high SNR regime. It is also seen that the signal strength of BFSS transceiver is discounted compare to that of using MF transceiver. The discount factor is determined by the angle subtended by vector $\mathbf{e}_1 = [1 \; 0 \; \cdots \; 0]^T$ and the null subspace in (33). The size of this angle in turn depends

on the dimension of the null space. But the null space's dimension is limited by the number of interference signals to be suppressed, given fixed M. The more interferers there are, the "smaller" the null space, resulting in small signal strength. The BFSS transceiver trades signal strength for zero interference.

4 DoA estimation

From analyses in the above sections, we know that DoA information of MS k, i.e., the elevation angle θ_k and the azimuth angle γ_k are "encoded" in the series expansions of its channel coefficient $h_k(\rho, \varphi)$. These information can be extracted by taking correlations of received signals. This extracted DoA only reveals in which direction a MS's signal comes from, and under LoS, this is also the direction a MS locates with respect to the LIS. To pinpoint a MS's position, a third coordinate, the distance ρ_k from the origin have to be determined. This can be achieved by utilizing off-the-shelf algorithm to estimate this distance [27–29]. This problem is well studied in literature, and thus we assumed the distances between the LIS and MSs are known in the following.

During training phase, each MS transmits a pilot symbol $\bar{s}_k$ with power that is proportional to square of its distance to the LIS, which makes received signal power levels from different MSs more or less the same. Then, the received aggregate signal at the LIS is given by

$$r_0(\theta_0, \gamma_0) = \frac{1}{2\pi R^2} \int_{\mathcal{D}} \sum_{k=1}^{K} g_k(\rho, \varphi) h_0(\rho, \varphi) \bar{s}_k \rho d\rho d\varphi + n_0, \tag{37}$$

where $h_0(\rho, \varphi) = \frac{4\pi}{\lambda} e^{-j\frac{2\pi}{\lambda}\rho \sin(\theta_0)\cos(\varphi-\gamma_0)}$ and the aggregate noise n_0 follows a white Gaussian distribution of mean zero and variance σ_0. The integration is normalized by area of the LIS to get succinct expressions in the following. Since MSs reside on one side of the LIS, the scanning variables θ_0 and γ_0 and directional angles of MSs are physically constrained by

$$\theta_0, \theta_k \in \left(0, \frac{\pi}{2}\right), \quad \gamma_0, \gamma_k \in [0, 2\pi). \tag{38}$$

Following similar derivations in Sect. 3, we have

$$r_0(\theta_0, \gamma_0) = \sum_{k=1}^{K} \frac{J_1(2\pi R\Delta(0,k)/\lambda)}{2\pi R\Delta(0,k)/\lambda} + n_0, \tag{39}$$

where

$$\Delta(0,k) = \sqrt{\sin^2\theta_0 + \sin^2\theta_k - 2\sin\theta_0 \sin\theta_k \cos(\gamma_0 - \gamma_k)}.$$

From Eq. (39), we see that the received signal is a sum of functions of the same form $\frac{J_1(x)}{x}$ with different arguments and noise. As Fig. 2 shows, this function oscillates with decaying envelop amplitude. At $x = 0$, it achieves maximum value of $\lim_{x\to 0} \frac{J_1(x)}{x} = \frac{1}{2}$. Each transmitting MS "excites" a waveform $\frac{J_1(x)}{x}$ in the received signal, and a "peak" appears at (θ_k, γ_k) if the argument $\Delta(0,k) = 0$ corresponding to $\theta_0 = \theta_k,\ \gamma_0 = \gamma_k$. This is shown by the following lemma.

Lemma 1 *Under the condition* (38), *the projected distance function* $\Delta(0,k)=0$ *if and only if* $\theta_0=\theta_k$ *and* $\gamma_0=\gamma_k$, *for some* k.

Proof See Appendix C. □

This lemma establishes the correspondence between $\Delta(0,k)=0$ and the scanning variables θ_0 and γ_0 equaling to the directional angles of some MS, i.e., $\theta_0=\theta_l$ and $\gamma_0=\gamma_l$ for some l. Hence, we can locate the "peak" signals to estimate DoAs of respective MSs. The accuracy of this DoA estimation process is affected by side lobes induced by interfering MSs.

Proposition 5 *DoA of MSs, i.e.,* θ_k *and* γ_k, *for* $k=1,2,\cdots,K$, *can be estimated by locating the peaks of function* $r_0(\theta_0,\gamma_0)$, $\theta_0\in\left(0,\frac{\pi}{2}\right)$, $\gamma_0\in[0,2\pi)$. *The estimation resolution is given by*

$$Res=\frac{\lambda a_{1m}}{2\pi R}, \tag{40}$$

where a_{1m} *is the m-th zero of* $J_1(x)$, $m=1,2,3,\cdots$.

The major source of interference of the proposed DoA estimation method comes from side lobes of $\frac{J_1(x)}{x}$ induced by MSs. Farther-away side lobes are smaller in amplitude and produces smaller disturbance. Selecting m in Proposition 5 is to determine how much disturbance will be considered acceptable. Larger m results in smaller disturbance and thus higher estimation accuracy. This leads to a trade-off between accuracy and resolution in the proposed estimation method, given other parameters fixed. As shown in Proposition 5, the resolution is inverse proportional to m. Increasing m increases a_{1m} and decreases the resolution. At the same time, inter-user projected distances are increased. The farther away from each other the MSs are, the smaller the mutual interference. As a result, estimation accuracy increases. Two other important parameters that also affect the resolution are R and λ. Larger R and/or smaller λ results in higher resolution. However, size of the LIS R cannot get too large due to physical constraint. It is more promising to employ high-frequency carriers to obtain high estimation resolution, since mmWave and higher spectra are to be employed in future wireless communication systems [30, 31].

Algorithm 1 Proposed DoA Estimation Algorithm

```
Input: r_0(θ_0, γ_0), for θ_0 ∈ (0, π/2), γ_0 ∈ [0, 2π)
for l = 1 to K do
    (θ_l, γ_l) = argmax_(θ_0,γ_0) r_0(θ_0, γ_0)
    η_l(θ_0, γ_0) = J_1(2πRΔ(0,l)/λ) / (2πRΔ(0,l)/λ);
    r_0(θ_0, γ_0) ← r_0(θ_0, γ_0) − η_l(θ_0, γ_0);
end for
return (θ_l, γ_l), l = 1, ···, K.
```

Algorithm 1 is proposed based on Proposition 5. The algorithm evaluates aggregate signal strength at different locations and obtains a location with maximum signal value as a DoA estimation for some MS. Then, the MS's signal is regenerated using the estimated DoA and subtracted from $r_0(\theta_0, \gamma_0)$. The major part of complexity comes from these evaluations. Thus, the complexity is proportional to $\frac{2\pi K}{Res}$. In the above discussion, a one-symbol training scheme is assumed. This can be easily generalized to multiple training symbols. Estimation accuracy can be improved by exploiting diversity among different received symbols.

5 Numerical results

In this section, simulation results are presented to show the performance of using circular LIS for communicating and DoA estimation.

5.1 Capacity

In the following numerical evaluations of sum rates, the scenario is that a LIS is installed on a building surface, serving MSs down on streets with LoS channels. The MSs' distance to the LIS is set to be larger than the Rayleigh distance $2(2R)^2/\lambda$. Since the LIS covers terminals in front of the antenna surface, the elevation angle is within the range $\theta_k \in (0, \pi/2)$ and azimuth angle is $\gamma_k \in [0, 2\pi)$, $k = 1, 2, \cdots, K$. These location coordinates are generated uniformly randomly in following simulations. Since each MS has a different received SNR, we define a reference SNR as rSNR $= \frac{P\lambda^2}{4\bar{\rho}\sigma^2}$, where $\bar{\rho}$ is the distance from a reference point to the LIS. This reference distance is set to be in the middle of the range.

MF beamformer performances are shown in Figs. 3 and 4. Figure 3 shows sum rates achieved by MF beamformer under different sets of configuration parameters. The performance plotted in the figure is averaged over the random Point-Process (PP), marked as "PP-averaged". From the figure, we see that the sum rate is increasing with SNR. Another observation is that larger LIS radius, i.e., larger aperture, result in better performance, corroborating analysis in Sect. 3.1. Simulation results of sum rate versus the number of MSs K are presented in Fig. 4. The sum rate is in general increasing with the number of MSs K. But the increasing rate becomes slower as K increases, because more simultaneous transmitting MSs result in an interference-limited system, showing saturated performance.

Figure 5 illustrates the performance of BFSS beamformer under various configurations. The sum rate is larger with larger LIS radius R and/or more number of MSs. These are the same as observed in MF receiver. An interesting observation is that with BFSS, increasing the carrier wavelength λ slightly increases sum rate, in contrast to what happens in MF receiver. This is indeed the case because BFSS suppresses inter-user interferences and its SNR is proportional to λ. In MF, increasing λ reduces the projected distance between MSs, which results in stronger interference.

Another important question is to compare performance between MF and BFSS beamformers, which is shown in Fig. 6. Under the same setting, MF performs better than BFSS in low SNR regime, but is inferior in high SNR. There is a point where BFSS surpasses MF in performance. After this cross point, MF sum rate saturates, as it enters

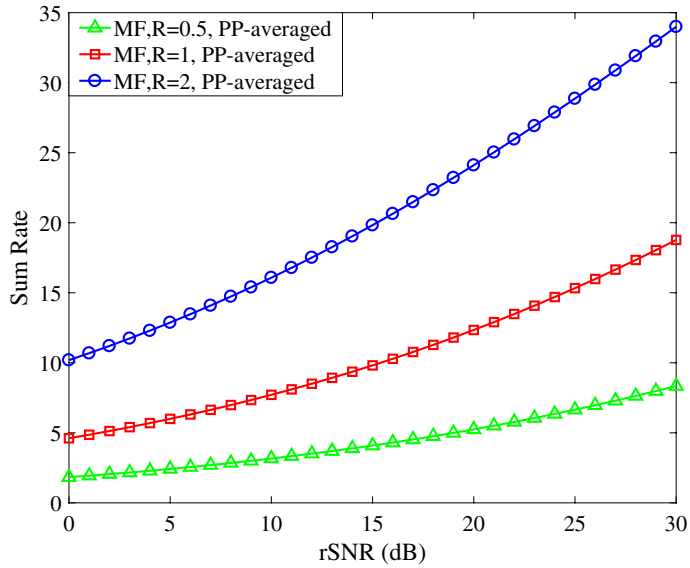

Fig. 3 Sum rate vs. SNR with MF transceiver. Parameters are set as $K = 10$, λ=0.3 m. 'PP-averaged' curves are obtained by averaged over 300 runs

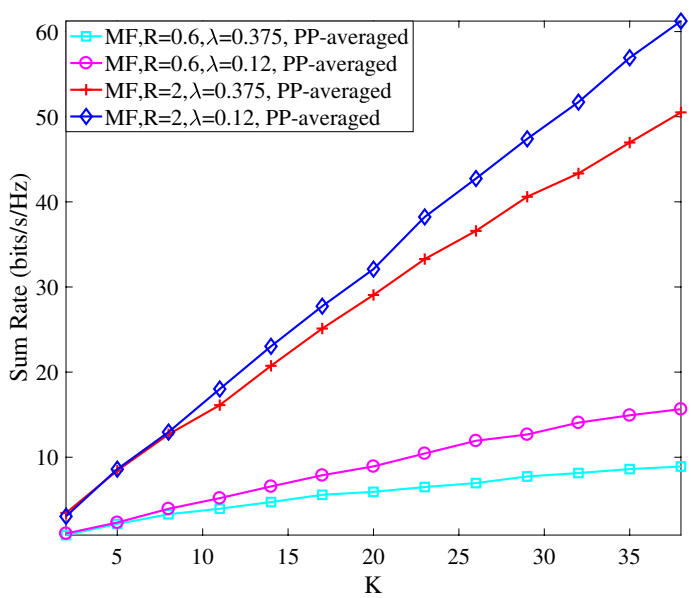

Fig. 4 Sum rate vs. number of MSs K with MF transceiver. Parameters are set as rSNR=10 dB. 'PP-averaged' curves are obtained by averaged over 300 runs

an interference-limited regime. The performance gap between BFSS and MF becomes larger and larger. This shows the promising performance gain of BFSS transceiver for interference-limited wireless networks. And as is envisioned, future cellular networks will be deeply interference-limited with massive connections and aggressive spectrum reuse schemes [32, 33].

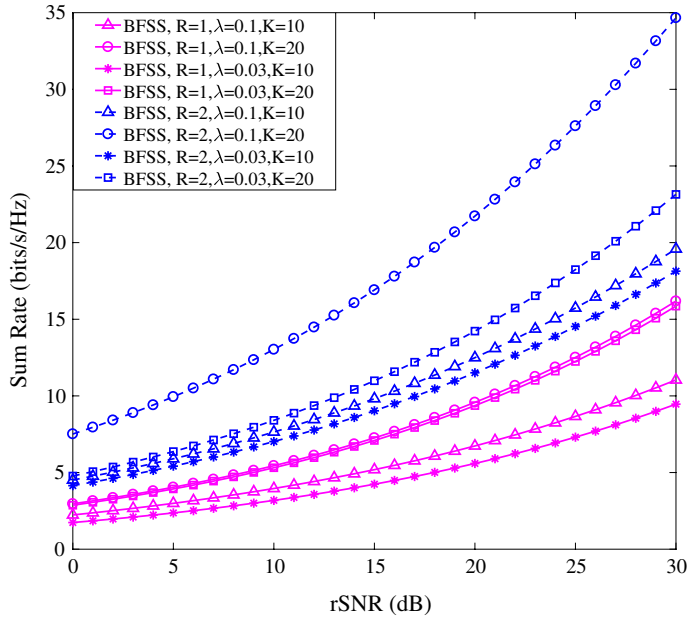

Fig. 5 Sum rate vs. rSNR with BFSS transceiver. Results are obtained by averaged over 300 runs

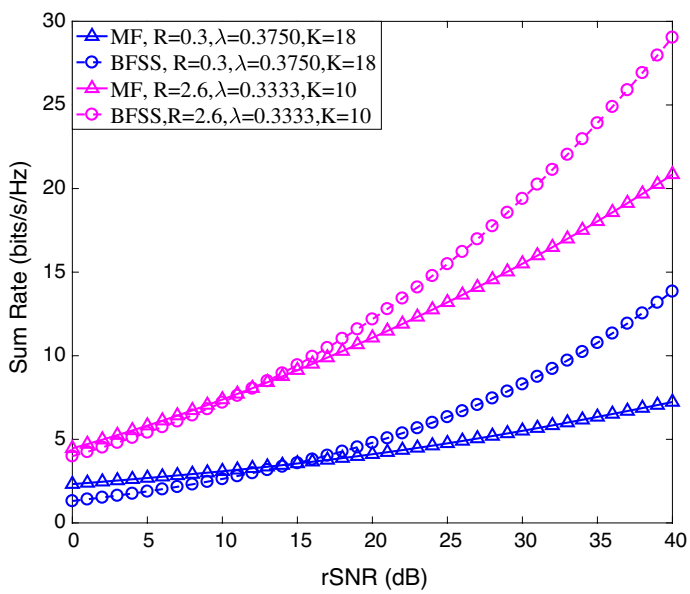

Fig. 6 Sum rate comparisons between MF and BFSS transceivers

In the development of BFSS beamformer in Proposition 3, we truncate the Bessel and Fourier series and keep M terms. It is important to investigate the effects of such truncation on overall performance. To this aim, Fig. 7 presents sum rate versus the number of truncated terms M. We see that, as M increases, the sum rate first increases and then decreases, resulting in a maximum value for each parameter setting. This is due to two conditions imposing on M has competing effects on the resultant beamformer, specifically, on the first coefficient of the BFSS beamformer, as shown in Proposition 4. The two

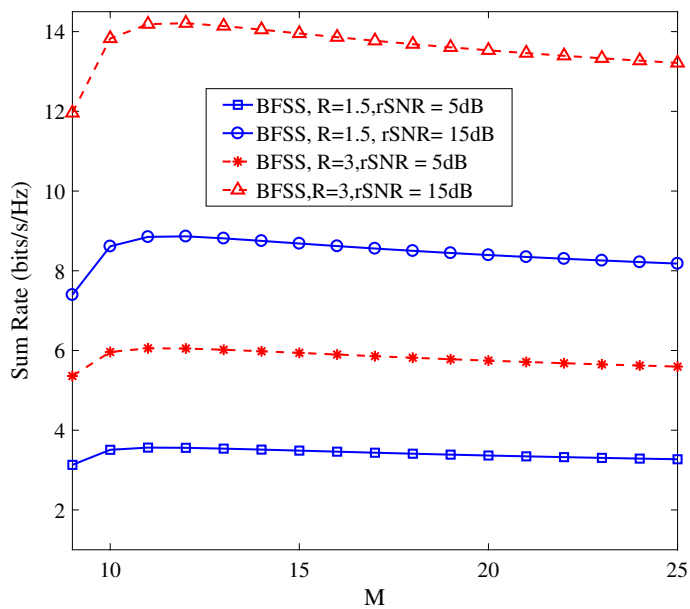

Fig. 7 Sum rate vs. M with BFSS transceiver. Number of MSs $K = 9$. $\lambda = 0.3$m. Results are obtained by averaged over 300 runs

conditions on M are Eqs. (23) and (29), corresponding to the normalization and interference-suppression requirements. On one hand, the normalization condition dictates that M coefficients of the BFSS beamformer have a fixed power. Increasing the number of coefficients reduces the power each one might get. On the other hand, the interference-suppression condition demands that M is large enough to cancel all interferers' signals. In the setting of Fig. 7, M must be larger than 8. Increasing M enlarges the null space of the interferers' signals, as shown in Eq. (33), which might result in large coefficient values. But, the coefficient values are also constrained by the normalization condition. The overall result of these two effects is shown in Fig. 7.

5.2 DoA estimation

In LoS environment, DoA reveals a MS's directional information of its position and also determines the phase of its channel coefficient to the LIS. In addition, estimating DoA under this scenario is part of the positioning procedure. The acquired DoA information can also be used in beamforming designs.

Figure 8 illustrates the function $r_0(\theta_0, \gamma_0)$ with three MSs and LIS radius $R = 1.5$ and carrier wavelength $\lambda = 0.1$m. The three "peaks" represents three signals present in the system. The coordinates of those "peaks" approximate the elevation and azimuth angles of corresponding signal's DoA. The approximation error mainly comes from tail fluctuation of the function $\frac{J_1(x)}{x}$ (refer to Eq. (39)), induced by presence of other MSs' transmitting signals. When two MSs' projected distance $\Delta(k_1, k_2)$ is larger than, e.g., a_{12}, the second zero of $\frac{J_1(x)}{x}$, the estimation error can be greatly reduced if parameters R and λ are large enough.

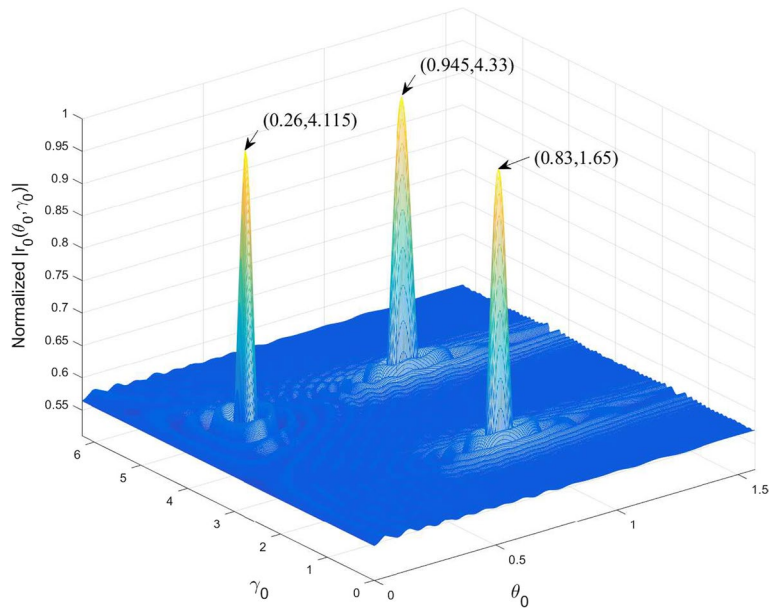

Fig. 8 Illustration of function $|r_0(\theta_0, \gamma_0)|$. Parameters are set as: $K = 3$, $R = 1.5$, $\lambda = 0.1$m, rSNR=5dB. Three MSs' DoAs are shown in the figure

To evaluate the proposed algorithm's performance, we run simulations for different parameters and present the Mean Square Error (MSE) vs the number of MSs K in Fig. 9. We see that MSE increases with K, and increases only slightly when K is larger than ten. More MSs transmitting signals result in more interference in the estimation process, increasing the MSE. But the increasing rate becomes small. Comparing different curves in the figure shows that large value of radius R and small wavelength λ improve the proposed estimation algorithm's performance. This is in

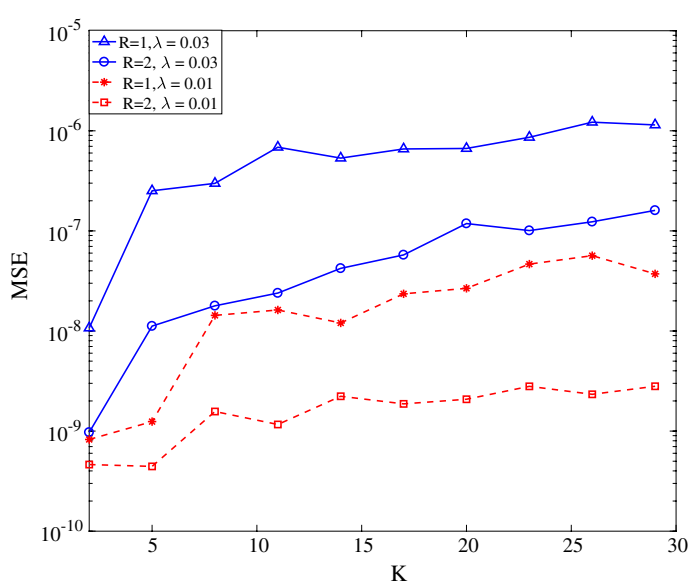

Fig. 9 Performance of the proposed DoA estimation. Averaged over 300 runs. rSNR=5dB

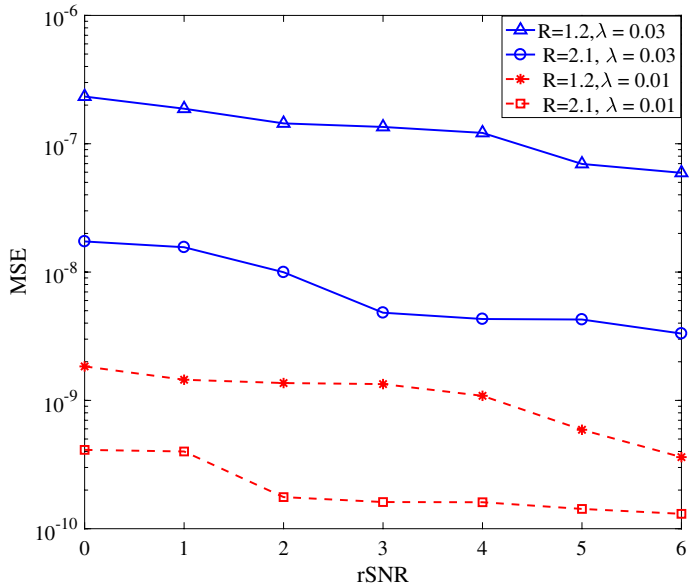

Fig. 10 Performance of the proposed DoA estimation. Averaged over 300 runs. $K = 5$

accordance with that large aperture and high-frequency carriers improve resolution. Importantly, for $R = 2$ and $\lambda = 0.01$m the MSE can be as low as about 10^{-9}. This wavelength corresponds to frequency of 30GHz. This is about in the lower part of the mmWave spectrum, which will be employed in future wireless communication systems [30, 31]. Figure 10 presents how the MSE performance varies with the rSNR. It is seen that as signal strength increases and/or noise power reduces, MSE decreases slightly.

6 Conclusion

This paper proposes a new interference-suppression transceiver for LoS multi-user LIS systems based on exploiting the signal structures resulting from geometric symmetries of the antenna surface. The signal can be decomposed into orthogonal communication modes using Bessel and Fourier series. The proposed beamformer tunes the coefficients of these communication modes to cancel inter-user interferences. The proposed transceiver method BFSS's performance is studied under varying parameters and compared with conventional MF receiver. The BFSS performs better than the MF in the high SNR regime. Another interesting result is that choosing more communication modes will not always increase the sum rate because power is thinly spread on these modes. Thus, we need to choose just enough modes but not too many. A DoA estimation method is also proposed for identifying directional information of MSs in LoS condition, following the same line of ideas. This method is demonstrated to have promising performance with high-frequency carriers, e.g., mmWave. The principle can be generalized to other symmetric geometries.

Appendix A: proof of proposition 1

The received signal for MS l can then be calculated as

$$\begin{aligned} r_l &= \int_{\mathcal{D}} g_l(\rho,\varphi) \sum_{k=1}^{K} f_k^{(MF)}(\rho,\varphi) s_k \rho d\rho d\varphi + n_l \\ &= \frac{\lambda}{4\pi} \frac{1}{\sqrt{\pi}R} \frac{s_l}{\rho_l} \int_0^R \int_0^{2\pi} \rho d\rho d\varphi \\ &\quad + \frac{\lambda}{4\pi} \frac{1}{\sqrt{\pi}R} \sum_{k\neq l} \frac{s_k}{\rho_l} \int_{\mathcal{D}} h_l(\rho,\varphi) h_k^*(\rho,\varphi) \rho d\rho d\varphi + n_l \\ &= \frac{\lambda}{4\sqrt{\pi}\rho_l} R s_l + \frac{\lambda}{2\sqrt{\pi}} R \sum_{k\neq l} \frac{1}{\rho_l} \Phi_{lk} s_k + n_l. \end{aligned}$$

The normalized effective channel coefficients Φ_{lk}, $k \neq l$, can be calculated as

$$\begin{aligned} \Phi_{lk} &\triangleq \frac{1}{2\pi R^2} \int_{\mathcal{D}} h_l(\rho,\varphi) h_k^*(\rho,\varphi) \rho d\rho d\varphi \\ &= \frac{1}{2\pi R^2} \int_{\mathcal{D}} e^{j\frac{2\pi}{\lambda}\rho \sin\theta_l \cos(\varphi-\gamma_l)} e^{-j\frac{2\pi}{\lambda}\rho \sin\theta_k \cos(\varphi-\gamma_k)} \rho d\rho d\varphi \\ &= \frac{1}{2\pi R^2} \int_{\mathcal{D}} e^{j\frac{2\pi}{\lambda}\rho[\sin\theta_l \cos(\varphi-\gamma_l) - \sin\theta_k \cos(\varphi-\gamma_k)]} \rho d\rho d\varphi \qquad (41) \\ &= \frac{1}{2\pi R^2} \int_0^R \int_0^{2\pi} e^{j\frac{2\pi}{\lambda}\rho\Delta(k,l)\cos(\varphi-\alpha_{kl})} \rho d\rho d\varphi \\ &= \frac{1}{R^2} \int_0^R J_0\left(\frac{2\pi}{\lambda}\rho\Delta(k,l)\right) \rho d\rho \end{aligned}$$

$$= \frac{\lambda}{2\pi R\Delta(k,l)} J_1\left(\frac{2\pi R\Delta(k,l)}{\lambda}\right). \qquad (42)$$

where step (41) follows from equation $J_n(x) = \frac{j^{-n}}{2\pi} \int_0^{2\pi} e^{j(x\cos\varphi + n\varphi)} d\varphi$ [34]. In above formulas, the normalized projected distance $\Delta(k,l)$ between MS k and l is defined by

$$\begin{aligned} &\Delta^2(k,l) \\ =&(\sin\theta_l \cos\gamma_l - \sin\theta_k \cos\gamma_k)^2 + (\sin\theta_l \sin\gamma_l - \sin\theta_k \sin\gamma_k)^2 \\ =&\sin^2\theta_k \cos^2\gamma_k - 2\sin\theta_k \cos\gamma_k \sin\theta_l \cos\gamma_l \\ &+ \sin^2\theta_l \cos^2\gamma_l + \sin^2\theta_k \sin^2\gamma_k \\ &- 2\sin\theta_k \sin\gamma_k \sin\theta_l \sin\gamma_l + \sin^2\theta_l \sin^2\gamma_l \\ =&\sin^2\theta_k + \sin^2\theta_l - 2\sin\theta_k \sin\theta_l \cos(\gamma_k - \gamma_l). \end{aligned} \qquad (43)$$

Appendix B: proof of proposition 3

Substituting (22) into (24), the received signal at MS l is given by

$$r_l = \sum_k s_k \int_{\mathcal{D}} g_l(\rho,\varphi) h_k^*(\rho,\varphi) \sum_{m=1}^{\infty} c_{km} J_\nu\left(a_{\nu m}\frac{\rho}{R}\right) e^{j(m-1)\varphi} \rho d\rho d\varphi + n_l. \tag{44}$$

In (44), the summation term can be computed as follows. When $k = l$, we have

$$\begin{aligned}
&\int_{\mathcal{D}} g_l(\rho,\varphi) h_l^*(\rho,\varphi) \sum_{m=1}^{\infty} c_{lm} J_\nu\left(a_{\nu m}\frac{\rho}{R}\right) e^{j(m-1)\varphi} \rho d\rho d\varphi \\
=&\frac{\lambda}{4\pi\rho_l} \sum_m c_{lm} \int_{\mathcal{D}} J_\nu\left(a_{\nu m}\frac{\rho}{R}\right) e^{j(m-1)\varphi} \rho d\rho d\varphi \\
=&\frac{\lambda}{4\pi\rho_l} \sum_m c_{lm} \int_0^R J_\nu\left(a_{\nu m}\frac{\rho}{R}\right) \rho d\rho \int_0^{2\pi} e^{j(m-1)\varphi} d\varphi \\
=&\frac{\lambda}{2\rho_l} c_{l1} \int_0^R J_\nu\left(a_{\nu 1}\frac{\rho}{R}\right) \rho d\rho.
\end{aligned}$$

Without loss of generality, let $\nu = 0$. Then,

$$\begin{aligned}
&\int_0^R J_0\left(a_{01}\frac{\rho}{R}\right) \rho d\rho \\
=&\frac{R^2}{a_{01}^2} \int_0^{a_{01}} J_0(\rho') \rho' d\rho' \\
=&\frac{R^2}{a_{01}^2} J_1(\rho')\rho' \Big|_0^{a_{01}} = \frac{R^2}{a_{01}} J_1(a_{01}).
\end{aligned}$$

When $k \neq l$, we have

$$\begin{aligned}
&\int_{\mathcal{D}} g_l(\rho,\varphi) h_k^*(\rho,\varphi) \sum_{m=1}^{\infty} c_{km} J_\nu\left(a_{\nu m}\frac{\rho}{R}\right) e^{j(m-1)\varphi} \rho d\rho d\varphi \\
=&\frac{\lambda}{4\pi\rho_l} \int_{\mathcal{D}} h_l(\rho,\varphi) h_k^*(\rho,\varphi) \sum_{m=1}^{\infty} c_{km} J_\nu\left(a_{\nu m}\frac{\rho}{R}\right) e^{j(m-1)\varphi} \rho d\rho d\varphi \\
=&\frac{\lambda}{4\pi\rho_l} \int_{\mathcal{D}} \sum_{m=1}^{\infty} c_{km} J_\nu\left(a_{\nu m}\frac{\rho}{R}\right) \\
&\quad \times e^{j\frac{2\pi}{\lambda}\rho[\sin\theta_l\cos(\varphi-\gamma_l)-\sin\theta_k\cos(\varphi-\gamma_k)]+j(m-1)\varphi} \rho d\rho d\varphi \\
=&\frac{\lambda}{4\pi\rho_l} \int_{\mathcal{D}} \sum_{m=1}^{\infty} c_{km} J_\nu\left(a_{\nu m}\frac{\rho}{R}\right) \\
&\quad \times e^{j\frac{2\pi}{\lambda}\rho\Delta(k,l)\cos(\varphi-\alpha_{kl})+j(m-1)\varphi} \rho d\rho d\varphi \\
=&\frac{\lambda}{2\rho_l} \sum_{m=1}^{\infty} j^{m-1} c_{km} e^{j(m-1)\alpha_{kl}} \\
&\quad \times \int_0^R J_\nu\left(a_{\nu m}\frac{\rho}{R}\right) J_{m-1}\left(\frac{2\pi}{\lambda}\rho\Delta(k,l)\right) \rho d\rho,
\end{aligned}$$

where α_{kl} is defined as in (28).

Evoking upper bounds given in [35], the integration in the above equation can be bounded as

$$\begin{aligned}&\int_0^R J_\nu\left(a_{\nu_m}\frac{\rho}{R}\right)J_{m-1}\left(\frac{2\pi}{\lambda}\rho\Delta(k,l)\right)\rho d\rho\\ <&\beta_0\beta_1\left(\frac{R}{a_{\nu m}}\right)^{1/3}(m-1)^{-\frac{1}{3}}\int_0^R \rho^{-\frac{1}{3}}\rho d\rho\\ =&\frac{3\beta_0\beta_1R^2}{5a_{\nu m}^{1/3}}(m-1)^{-\frac{1}{3}},\qquad \nu\geqslant 0, m-1>0,\end{aligned}$$

where $\beta_0 = 0.674885...$ and $\beta_1 = 0.7857$ are constants [35]. As order m increases, the integration approaches zero. When $m > M \triangleq \max\{K, R^3\}$, the above integration can be omitted.

Collecting the above results together, equation (44) can be rewritten as

$$r_l = \frac{\lambda}{2\rho_l}c_{l1}\xi_\nu s_l + \frac{\lambda}{2\rho_l}\sum_{k\neq l}s_k\sum_{m=1}^{M}c_{km}\zeta_{lkm} + n_l, \tag{45}$$

where

$$\xi_\nu = \int_0^R J_\nu\left(a_{\nu 1}\frac{\rho}{R}\right)\rho d\rho, \tag{46}$$

and

$$\begin{aligned}\zeta_{lkm} =& j^{m-1}e^{j(m-1)\alpha_{kl}}\\ &\times\int_0^R J_\nu\left(a_{\nu_m}\frac{\rho}{R}\right)J_{m-1}\left(\frac{2\pi}{\lambda}\rho\Delta(k,l)\right)\rho d\rho.\end{aligned} \tag{47}$$

and

$$\alpha_{kl} \triangleq \arctan\left\{\frac{\sin\theta_l\sin\gamma_l - \sin\theta_k\sin\gamma_k}{\sin\theta_l\cos\gamma_l - \sin\theta_k\cos\gamma_k}\right\}. \tag{48}$$

Appendix C: proof of lemma 1

If $\theta_0 = \theta_k$ and $\gamma_0 = \gamma_k$, then it is obvious $\Delta(0,k) = 0$.

If $\Delta(0,k) = 0$, then

$$\begin{aligned}&\sin^2\theta_0 + \sin^2\theta_k = 2\sin\theta_0\sin\theta_k\cos(\gamma_0-\gamma_k)\\ \Longleftrightarrow\ &\frac{\sin\theta_0}{\sin\theta_k} + \frac{\sin\theta_k}{\sin\theta_0} = 2\cos(\gamma_0-\gamma_k)\leqslant 2,\quad \theta_0,\theta_k\in\left(0,\frac{\pi}{2}\right)\end{aligned}$$

But, we have inequality $\frac{\sin\theta_0}{\sin\theta_k} + \frac{\sin\theta_k}{\sin\theta_0} \geqslant 2$, with equality being achieved when $\sin\theta_k = \sin\theta_0$. This equality condition in turn leads to $\gamma_0 = \gamma_k$.

Abbreviations

LIS	Large intelligent surface
LoS	Line-of-sight
DoA	Direction-of-arrival
MS	Mobile station
RIS	Reconfigurable intelligent surface
IRS	Intelligent reflecting surface
DoF	Degree-of-freedom
MMSE	Minimum mean-square error
BFSS	Bessel-and-Fourier-series synthesis
MF	Matched filter
MSE	Mean-square error
SNR	Signal-to-noise ratio

Acknowledgements
This work was supported by National Natural Science Foundation of China (61602317) and Natural Science Foundation of Guangdong Province (2016A030310066).

Author contributions
This work is all done by the author Jiayi Chen.

Funding
This research received no external funding.

Availability of data and materials
This manuscript has no associated dataset.

Declarations

Competing interests
The authors declare that they have no competing interests.

Received: 6 July 2023 Accepted: 18 November 2023
Published online: 12 December 2023

References

1. E. Björnson, L. Sanguinetti, H. Wymeersch, J. Hoydis, T.L. Marzetta, Massive mimo is a reality-what is next?: five promising research directions for antenna arrays. Dig. Sig. Process. **94**, 3–20 (2019)
2. J. Yuan, H.Q. Ngo, M. Matthaiou, Towards large intelligent surface (lis)-based communications. IEEE Trans. Commun. **68**(10), 6568–6582 (2020)
3. S. Hu, F. Rusek, O. Edfors, Beyond massive mimo: the potential of data transmission with large intelligent surfaces. IEEE Trans. Signal Process. **66**(10), 274–2758 (2018)
4. D. Dardari, Communicating with large intelligent surfaces: fundamental limits and models. IEEE J. Sel. Areas Commun. **38**(11), 2526–2537 (2020)
5. J. Hunt, T. Driscoll, A. Mrozack, G. Lipworth, M. Reynolds, D. Brady, D.R. Smith, Metamaterial apertures for computational imaging. Science **339**(6117), 310–313 (2013)
6. L. Li, T. Jun Cui, W. Ji, S. Liu, J. Ding, X. Wan, Y. Bo Li, M. Jiang, C.-W. Qiu, S. Zhang, Electromagnetic reprogrammable coding-metasurface holograms. Nat. Commun. **8**(11), 197 (2017)
7. C. Liaskos, S. Nie, A. Tsioliaridou, A. Pitsillides, S. Ioannidis, I. Akyildiz, A new wireless communication paradigm through software-controlled metasurfaces. IEEE Commun. Mag. **56**(9), 162–169 (2018)
8. N. Shlezinger, O. Dicker, Y.C. Eldar, I. Yoo, M.F. Imani, D.R. Smith, Dynamic metasurface antennas for uplink massive mimo systems. IEEE Trans. Commun. **67**(10), 6829–6843 (2019)
9. C.L. Holloway, E.F. Kuester, J.A. Gordon, J. O'Hara, J. Booth, D.R. Smith, An overview of the theory and applications of metasurfaces: the two-dimensional equivalents of metamaterials. IEEE Antennas Propag. Mag. **54**(2), 10–35 (2012)
10. A. Puglielli, N. Narevsky, P. Lu, T. Courtade, G. Wright, B. Nikolic, E. Alon, A scalable massive mimo array architecture based on common modules, in *Proceeding of IEEE International Conference on Communication Workshop (ICCW)*, June 2015, pp. 1310–1315
11. Q. Wu, R. Zhang, Intelligent reflecting surface enhanced wireless network via joint active and passive beamforming. IEEE Trans. Wireless Commun. **18**(11), 5394–5409 (2019)
12. Z. Zhang, L. Dai, A joint precoding framework for wideband reconfigurable intelligent surface-aided cell-free network. IEEE Trans. Signal Process. **69**, 4085–4101 (2021)
13. H.U. Rehman, F. Bellili, A. Mezghani, E. Hossain, Modulating intelligent surfaces for multi-user mimo systems: Beamforming and modulation design, arXiv:2108.10505, Aug 2021. [Online]. Available: http://arxiv.org/abs/2108.10505
14. D.A.B. Miller, Communicating with waves between volumes: evaluating orthogonal spatial channels and limits on coupling strengths. Appl. Opt. **39**(11), 1681–1699 (2000)
15. A. Poon, R. Brodersen, D. Tse, Degrees of freedom in multiple-antenna channels: a signal space approach. IEEE Trans. Inf. Theory **51**(2), 523–536 (2005)
16. N. Decarli, D. Dardari, Communication modes with large intelligent surfaces in the near field, arXiv:2108.10569, August 2021. [Online]. Available: http://arxiv.org/abs/2108.10569

17. S. Hu, F. Rusek, O. Edfors, Beyond massive mimo: the potential of positioning with large intelligent surfaces. IEEE Trans. Signal Process. **66**(7), 1761–1774 (2018)
18. M. Jung, W. Saad, Y. Jang, G. Kong, S. Choi, Performance analysis of large intelligent surfaces (liss): asymptotic data rate and channel hardening effects. IEEE Trans. Wireless Commun. **19**(3), 2052–2065 (2020)
19. M. Jung, W. Saad, G. Kong, Performance analysis of active large intelligent surfaces (liss): uplink spectral efficiency and pilot training. IEEE Trans. Commun. **69**(5), 3379–3394 (2021)
20. R. Jess Williams, P. Ramirez-Espinosa, E. de Carvalho, T.L. Marzetta, Multiuser mimo with large intelligent surfaces: communication model and transmit design, in *Proceeding on IEEE International conference on communications (ICC)*, June 2021, pp. 1–6
21. Z. Zhang, L. Dai, Continuous-aperture mimo for electromagnetic information theory, arXiv:2111.08630, November 2021.
22. T.S. Rappaport, E. Ben-Dor, J. N. Murdock, Y. Qiao, 38 ghz and 60 ghz angle-dependent propagation for cellular amp; peer-to-peer wireless communications, in *Proceeding of IEEE International Conference on Communications (ICC)*, 2012, pp. 4568–4573
23. A. Sayeed, Deconstructing multiantenna fading channels. IEEE Trans. Signal Process. **50**(10), 2563–2579 (2002)
24. R. Ertel, P. Cardieri, K. Sowerby, T. Rappaport, J. Reed, Overview of spatial channel models for antenna array communication systems. IEEE Pers. Commun. **5**(1), 10–22 (1998)
25. L.C. Andrews, *Special functions of mathematics for engineers*, 2nd edn. (McGraw-Hill Inc, New York city, 1992)
26. G.B. Arfken, H.J. Weber, F. Harris, *Mathematical methods for physicists: a comprehensive guide* (Academic Press, Cambridge, 2005)
27. A. Zanella, Best practice in RSS measurements and ranging. IEEE Commun. Surv. Tutor. **18**(4), 2662–2686 (2016)
28. K.-I. Itoh, S. Watanabe, J.-S. Shih, T. Sato, Performance of handoff algorithm based on distance and RSSI measurements. IEEE Trans. Veh. Technol. **51**(6), 1460–1468 (2002)
29. G. Ghatak, On the placement of intelligent surfaces for RSSI-based ranging in mm-wave networks. IEEE Commun. Lett. **25**(6), 2043–2047 (2021)
30. I.A. Hemadeh, K. Satyanarayana, M. El-Hajjar, L. Hanzo, Millimeter-wave communications: physical channel models, design considerations, antenna constructions, and link-budget. IEEE Commun. Surv. Tutor. **20**(2), 870–913 (2018)
31. B. Ning, Z. Tian, Z. Chen, C. Han, J. Yuan, S. Li, Prospective beamforming technologies for ultra-massive mimo in terahertz communications: a tutorial, [Online]. arXiv:2107.03032, (2021)
32. W. Nam, D. Bai, J. Lee, I. Kang, Advanced interference management for 5g cellular networks. IEEE Commun. Mag. **52**(5), 52–60 (2014)
33. B. Soret, K.I. Pedersen, N.T.K. Jørgensen, V. Fernández-López, Interference coordination for dense wireless networks. IEEE Commun. Mag. **53**(1), 102–109 (2015)
34. G. Arfken, H. Weber, *Mathematical methods for physicists*, 7th edn. (Academic press, Cambridge, 2013)
35. L.J. Landau, Bessel functions: monotonicity and bounds. J. Lond. Math. Soc. **61**(1), 197–215 (2000)

Publisher's Note